Polarized image of an equatorial emitting ring around a Konoplya-Zhidenko rotating non-Kerr black hole*

Xin Qin (秦欣)[1,2†] Fen Long (龙芬)[3‡] Songbai Chen (陈松柏)[4,5§] Jiliang Jing (荆继良)[4,5¶]

[1]School of Physics and Electronic Science, Hunan University of Science and Technology, Xiangtan 411021, People's Republic of China
[2]Key Laboratory of Intelligent Sensors and Advanced Sensing Materials of Hunan Province, Hunan University of Science and Technology, Xiangtan 411021,People's Republic of China
[3]School of Mathematics and Physics, University of South China, Hengyang, 421001, People's Republic of China
[4]Department of Physics, Institute of Interdisciplinary Studies, Synergetic Innovation Center for Quantum Effects and Applications, Hunan Normal University, Changsha 410081, Hunan, People's Republic of China
[5]Center for Gravitation and Cosmology, College of Physical Science and Technology, Yangzhou University, Yangzhou 225009, People's Republic of China

Abstract: We investigate the polarized images of an equatorial emitting ring around a rotating Konoplya-Zhidenko non-Kerr black hole, which incorporates an additional deformation parameter. This deformation parameter, η, permits the spin parameter to exceed the upper bound imposed by the standard Kerr black hole. Our results indicate that the polarized images depend not only on the magnetic field configuration, fluid velocity, and observer inclination angle, but also on the spin and deformation parameters. As the deformation parameter increases, the polarization intensity decreases monotonically. Conversely, the magnitude of the Electric Vector Position Angle (EVPA) increases with η. Furthermore, we observe that η may induce subtle yet discernible azimuthal separation features, potentially distinguishing its effects from those of the spin parameter and the magnetic field orientation angle. Nevertheless, these features remain difficult to resolve under current observational conditions and will require verification by future high-resolution facilities such as the next-generation Event Horizon Telescope (ngEHT).

Keywords: Polarized image, Non-Kerr black hole, Deformation parameter

DOI: 10.1088/1674-1137/ae740c **CSTR:**

I. INTRODUCTION

The Event Horizon Telescope (EHT) Collaboration has released images of the supermassive black holes at the centers of M87 and Sgr A* [1−7], ushering in a new era in black hole astrophysics. Recently, polarized images of these black holes have also been published [8−10], providing the first measurements of polarization information reflecting magnetic field properties in such close proximity to their event horizons. These images exhibit strong, highly ordered spiral polarization patterns, suggesting that analogous magnetic field configurations may exist in the vicinity of these supermassive black holes.

Studies indicate that the formation of polarization patterns depends not only on the physical properties of the accretion disk but also on the curved spacetime structure near the black hole. Consequently, investigations of black hole polarization images provide new insights into both the mechanisms underlying powerful jet formation and the physical properties of black holes. Furthermore, they serve as a means to test alternative theories of gravity.

Numerical simulations are typically employed to accurately model polarized images of black holes. However, such simulations entail substantial computational costs, primarily due to the need for extensive parameter surveys and the complex coupling between astrophysical and relativistic effects. To mitigate these costs, Narayan et al. recently proposed a simplified radiative fluid ring model on the equatorial plane of a black hole to study the polarized images of Schwarzschild black holes [11]. This model can reproduce the polarization features

Received 2 March 2026; Accepted 28 May 2026

* This work was supported by the National Natural Science Foundation of China (Grant Nos. 12405053, 12275078, 12205140, 11875026, 12035005, 2020YFC2201400), the Natural Science Foundation of Hunan Province (Grant Nos. 2024JJ6211, 2023JJ40523), and the Scientific Research Fund of Hunan Provincial Education Department (Grant No. 24C0229)

† E-mail: qx@hnust.edu.cn
‡ E-mail: lf@usc.edu.cn
§ E-mail: csb3752@hunnu.edu.cn
¶ E-mail: jljing@hunnu.edu.cn

observed in the M87* images released by the Event Horizon Telescope. A notable feature of this model is its ability to decouple and analyze the individual effects of various physical factors on polarized images, such as the magnetic field configuration around the black hole, the velocity profile of the accretion flow, and the observation inclination angle. The model was subsequently extended to more realistic scenarios involving rotating Kerr black holes [12], demonstrating that the differences in simulated images of the M87* black hole under low-spin and high-spin conditions primarily stem from differences in accretion dynamics. More recently, polarized images of black holes have been further investigated [13−23].

Although Einstein's general relativity has passed numerous observational and experimental tests, current results are still insufficient to definitively rule out alternative theoretical models. Among these alternatives, Johannsen and Psaltis proposed a rotating non-Kerr spacetime metric that deviates from the Kerr metric [24] with the aim of testing the black hole no-hair theorem. Their spacetime incorporates an additional deformation parameter, alongside the mass and spin parameters, to quantify deviations from the standard Kerr black hole spacetime. Recently, Konoplya and Zhidenko proposed another rotating non-Kerr black hole metric with static deformation [25], which can be regarded as an axisymmetric vacuum solution of a yet-unknown alternative theory of gravity. Because the event horizon radius does not depend on the polar angle, the horizon surface in this spacetime remains spherical, similar to the Kerr case. It has been shown that for certain values of the deformation parameter, the quasinormal modes of the Konoplya-Zhidenko rotating non-Kerr black hole are identical to those of the Kerr black hole. This result provides strong support for the validity of such deformed black hole models. Furthermore, observational constraints from quasi-periodic oscillations [26] and the iron line [27] provide additional support for the hypothesis that this class of black holes can describe real astrophysical black holes. The physical properties and observational signatures of these rotating non-Kerr black holes have been extensively explored [28−32]. This paper aims to investigate the polarized images in the spacetime of the Konoplya-Zhidenko rotating non-Kerr black hole, analyzing the influence of the deformation parameter on the polarization intensity and the electric vector position angle (EVPA).

This paper is organized as follows: Section 2 introduces the Konoplya-Zhidenko rotating non-Kerr black hole spacetime and presents the formula for the observed polarization vector. Section 3 presents the polarized images of the equatorial emitting ring and analyzes the effects of the deformation parameter on the polarization intensity and the EVPA.

II. OBSERVED POLARIZATION FIELD IN A KONOPLYA-ZHIDENKO ROTATING NON-KERR BLACK HOLE

The Konoplya-Zhidenko rotating non-Kerr black hole solution, introduced in [25], describes a rotating black hole geometry that deviates from the Kerr solution through an additional deformation parameter. In Boyer-Lindquist coordinates, the metric takes the form

$$ds^2=-\frac{\Delta\rho^2}{\Xi}dt^2+\frac{\Xi\sin^2\theta}{\rho^2}(d\phi-\omega dt)^2+\frac{\rho^2}{\Delta}dr^2+\rho^2d\theta^2, \quad (1)$$

with

$$\Delta=r^2-2Mr+a^2-\frac{\eta}{r}, \quad (2)$$

$$\rho^2=r^2+a^2\cos^2\theta, \quad (3)$$

$$\omega=\frac{a(a^2+r^2-\Delta)}{\Xi}, \quad (4)$$

$$\Xi=\left(r^2+a^2\right)^2-\Delta a^2\sin^2\theta. \quad (5)$$

where M, a, and η denote the mass, spin, and deformation parameter, respectively. Compared to the Kerr black hole, the inclusion of the deformation parameter not only extends the permissible range of the spin parameter a but also modifies the spacetime structure within the strong-field regime. When $\eta=0$, the metric (1) reduces to the Kerr metric. In accordance with the weak cosmic censorship conjecture, we restrict our analysis to spacetimes in which an event horizon exists, thereby ensuring that Equation (1) describes a black hole geometry. The condition for the existence of an event horizon is given by:

$$\begin{cases}\eta>0, & (a>M)\\ \eta>-\dfrac{2}{27}\left(\sqrt{4M^2-3a^2}+2M\right)^2\left(\sqrt{4M^2-3a^2}-M\right), & (a<M)\end{cases} \quad (6)$$

If the parameters η and a fall within alternative ranges, the spacetime corresponds to a naked singularity.

To investigate the polarized images of the equatorial emitting ring in the Konoplya-Zhidenko rotating non-Kerr black hole spacetime, we first present the photon geodesic equation:

$$\frac{\rho^2}{E}p^t = \frac{r^2+a^2}{\Delta}\left(r^2+a^2-a\lambda\right)+a\left(\lambda-a\sin^2\theta\right),$$
$$\frac{\rho^2}{E}p^\phi = \frac{a}{\Delta}\left(r^2+a^2-a\lambda\right)+\frac{\lambda}{\sin^2\theta}-a,$$
$$\frac{\rho^2}{E}p^r = \pm_r\sqrt{\mathcal{R}(r)},$$
$$\frac{\rho^2}{E}p^\theta = \pm_\theta\sqrt{\Theta(\theta)}, \tag{7}$$

where $\mathcal{R}(r)$ and $\Theta(\theta)$ represent the radial and angular potentials, respectively, which take the form

$$\mathcal{R}(r) = \left(r^2+a^2-a\lambda\right)^2-\Delta\left[\eta+(a-\lambda)^2\right],$$
$$\Theta(\theta) = \eta+a^2\cos^2\theta-\lambda^2\cot^2\theta. \tag{8}$$

The radial integral I_r and the angular integral G_θ for a photon propagating along a null geodesic from an initial point $(r_s,\theta_s=\frac{\pi}{2})$ to a final point $(r_o\to\infty,\theta_o)$ are expressed as [33–35]:

$$I_r \equiv -\int_{r_s}^{r_o}\frac{dr}{\pm_r\sqrt{\mathcal{R}(r)}} = -\int_{\theta_s}^{\theta_o}\frac{d\theta}{\pm_r\sqrt{\Theta(\theta)}} \equiv G_\theta. \tag{9}$$

where the slash through the integral sign denotes that the sign of $\pm_r$ or $\pm_\theta$ reverses whenever the photon encounters a radial or angular turning point. For a photon trajectory with m turning points, the radial integral is expressed as:

$$G_\theta^m = \frac{1}{\sqrt{-u_-a^2}}\left(2mK\left(\frac{u_+}{u_-}\right)-sign(y)F_o\right). \tag{10}$$

Moreover, the relationship between (λ,η) and (x,y) is expressed as follows:

$$x = -\frac{\lambda}{\sin\theta_o}, \qquad y = \pm_o\sqrt{\Theta(\theta)}. \tag{11}$$

Based on Eqs.(9), (10), and (11), the celestial coordinates (x,y) at the observer's position can be computed numerically.

Consider a point source located on a radiation ring in the equatorial plane of the black hole. In the local orthonormal frame of a zero-angular-momentum observer (ZAMO) co-located with the source, the emitter's velocity vector lies entirely within the $\hat{r}-\hat{\phi}$ plane and takes the form:

$$\vec{\beta} = \beta_v\left[\cos\chi(\hat{r})+\sin\chi(\hat{\phi})\right]. \tag{12}$$

The four-momentum of the photon in the boosted orthonormal frame can be obtained

$$p^{(a)} = \Lambda^{(a)}_{\ (b)}\eta^{(b)(c)}e^{\mu}_{\ (c)}p_\mu. \tag{13}$$

where $e^{\mu}_{\ (c)}$ and $\Lambda^{(a)}_{\ (b)}$ are the zero-angular-momentum observer tetrad and the Lorentz transformation [12], respectively. Thus, in the boosted orthonormal frame, the polarization vector is given by the cross product of the momentum $\vec{p}$ and the magnetic field $\vec{B}$, and is expressed as:

$$f^{(t)} = 0, \qquad f^{(r)} = \frac{p^{(\phi)}\times B^{(\theta)}}{|\vec{p}|},$$
$$f^{(\theta)} = \frac{p^{(r)}\times B^{(\phi)}}{|\vec{p}|}, \qquad f^{(\phi)} = \frac{p^{(\theta)}\times B^{(r)}}{|\vec{p}|}. \tag{14}$$

In the fluid frame, the magnetic field can be expressed as:

$$\begin{aligned}\vec{B} &= B_r\hat{e}_r+B_\phi\hat{e}_\phi+B_\theta\hat{e}_\theta\\ &= B_{eq}(cos\epsilon\hat{e}_r+sin\epsilon\hat{e}_\phi)+B_\theta\hat{e}_\theta\\ &= \vec{B}_{eq}+B_\theta\hat{e}_\theta.\end{aligned} \tag{15}$$

Thus, by applying the inverse transformation, the polarization four-vector f^μ can be expressed as

$$f^\mu = e^{\mu}_{\ (b)}\Lambda^{(b)}_{\ (a)}f^{(a)}, \tag{16}$$

The polarization vector satisfies the normalization condition,

$$f^\mu f_\mu = \sin\zeta^2|\vec{B}|, \tag{17}$$

where ζ is the angle between the momentum $\vec{p}$ and the magnetic field $\vec{B}$. As photons propagate along the geodesic, the polarization vector f^μ obeys

$$f^\mu p_\mu = 0, \qquad p^\mu\nabla_\mu f^\nu = 0. \tag{18}$$

Since the rotating Konoplya-Zhidenko non-Kerr black hole ((1)) describes a type D spacetime, the conserved Penrose-Walker constant κ can be expressed as [36]

$$\kappa = p^i f_j(l_i n_j - l_j n_i - m_i\bar{m}_j+\bar{m}_i m_j)\Psi_2^{\left(-\frac{1}{3}\right)}. \tag{19}$$

with

$$\kappa = \kappa_1+i\kappa_2 = (A-iB)\Psi_2^{\left(-\frac{1}{3}\right)},$$
$$A = \left(p^t f^r-p^r f^t\right)+a\sin^2\theta\left(p^r f^\phi-p^\phi f^r\right),$$
$$B = \left[\left(r^2+a^2\right)\left(p^\phi f^\theta-p^\theta f^\phi\right)-a\left(p^t f^\theta-p^\theta f^t\right)\right]. \tag{20}$$

where Ψ_2 is the Weyl scalar, given explicitly by:

$$\Psi_2 = \frac{a\cos\theta\left(5\imath\eta r - 6\imath M r^3 + a\eta\cos\theta\right) - 2r^2\left(5\eta + 3Mr^2\right)}{6r^3\left(r - \imath a\cos^3\theta\right)^3\left(r + \imath a\cos\theta\right)}. \tag{21}$$

The Walker-Penrose conserved quantity relates the polarization states at the emission source to those measured by the observer. By combining the celestial coordinates (x,y) with this conserved quantity at the source, the observed polarization vector can be expressed as

$$f^x = \frac{y\kappa_2 - \mu\kappa_1}{\mu^2 + y^2}, \qquad f^y = \frac{y\kappa_1 + \mu\kappa_2}{\mu^2 + y^2}, \qquad \mu = -(x + a\sin\theta_o). \tag{22}$$

The observed intensity of linearly polarized synchrotron emission produced by hot gas near a black hole is denoted by

$$|I| = g^{3+\alpha_\nu} l_p |\vec{B}|^{1+\alpha_\nu} (sin\zeta)^{1+\alpha_\nu}, \tag{23}$$

where $g = \frac{E_o}{E_s}$ is the photon redshift between the source and the observer, and $l_p = \frac{p_s^{(t)}}{p_s^{(z)}} H$ is the geodesic path length through the emitting medium. The spectral index $\alpha_\nu = 1$ is determined by the properties of the accretion disk. Therefore, the observed polarization vector components are given by

$$\begin{aligned} f^x_{obs} &= \sqrt{l_p} g^2 |B| \sin\zeta f^x, \\ f^y_{obs} &= \sqrt{l_p} g^2 |B| \sin\zeta f^y. \end{aligned} \tag{24}$$

The total polarized intensity and EVPA on the observer's screen are given by

$$\begin{aligned} I &= \left(f^x_{obs}\right)^2 + \left(f^y_{obs}\right)^2, \\ \mathrm{EVPA} &= \frac{1}{2}\arctan\frac{\mathrm{U}}{\mathrm{Q}}, \end{aligned} \tag{25}$$

Here, Q and U denote the Stokes parameters.

$$Q = \left(f^y_{obs}\right)^2 - \left(f^x_{obs}\right)^2, \qquad U = -2 f^x_{obs} f^y_{obs}. \tag{26}$$

Within the Konoplya-Zhidenko rotating non-Kerr black hole spacetime, the polarization intensity and the electric vector position angle of a point source can be computed using the celestial coordinates (x,y) and Eqs.(19), (23)–(26). Repeating this procedure along the emitting ring reveals the influence of the deformation parameter on the overall polarization pattern.

III. EFFECTS OF THE DEFORMATION PARAMETER ON THE POLARIZED IMAGE IN THE KONOPLYA-ZHIDENKO ROTATING NON-KERR BLACK HOLE SPACETIME

In this section, we present the polarized image of an emitting ring with radius $r_s = 4.5$ surrounding a Konoplya-Zhidenko rotating non-Kerr black hole. This radius better matches the observational characteristics of M87* [11, 12]. The results show that the pattern of the polarized image depends not only on the deformation parameters but also on factors such as the black hole spin parameter, magnetic field structure, fluid velocity, and observer inclination angle. The deformation parameter not only modifies the spacetime geometry around the black hole but also extends the allowed range of the spin parameter beyond that of a standard Kerr black hole.

We investigate the influence of the deformation parameter on the polarized images of the equatorial emission ring for an equatorial magnetic field configuration, as shown in Figs. 1–4. We define the quantity $\Delta\mathrm{EVPA} \equiv \mathrm{EVPA} - \mathrm{EVPA}_{\eta=0.5}$. Figures 1–4 indicate that, for a fixed spin parameter a, the total polarized intensity I decreases monotonically with increasing η. According to Eqs. (23) and (24), the total polarized intensity is proportional to the fourth power of the redshift factor g. This strong dependence renders g the dominant factor governing the total polarized intensity. Consequently, we further investigate the impact of the deformation parameter on the redshift factor in Fig. 5. The results demonstrate that the redshift factor decreases significantly as η increases. This behavior can be attributed to the modification of the spacetime geometry induced by η. Specifically, η enters the time component of the metric (g_{tt}) as a positive term, effectively reducing the absolute value of g_{tt}. This modification alters the time dilation effect, thereby intensifying the gravitational redshift experienced by the photons. As a result, the redshift factor g decreases, leading to a reduction in the total polarized intensity I.

However, the dependence of the EVPA on the deformation parameter also varies with the magnetic field configuration. As illustrated in Figs. 1 and 2, the EVPA decreases monotonically for a purely radial magnetic field but exhibits non-monotonic behavior for a purely azimuthal magnetic field. Although the trends differ across magnetic field configurations, the fourth column reveals that the absolute value of ΔEVPA consistently increases with the deformation parameter. This behavior arises because the polarization vector $\vec{f}^{\mu}$ undergoes parallel transport along null geodesics as photons propagate through curved spacetime. Consequently, a greater degree of spacetime deformation results in a larger rotation of the polarization direction during propagation.

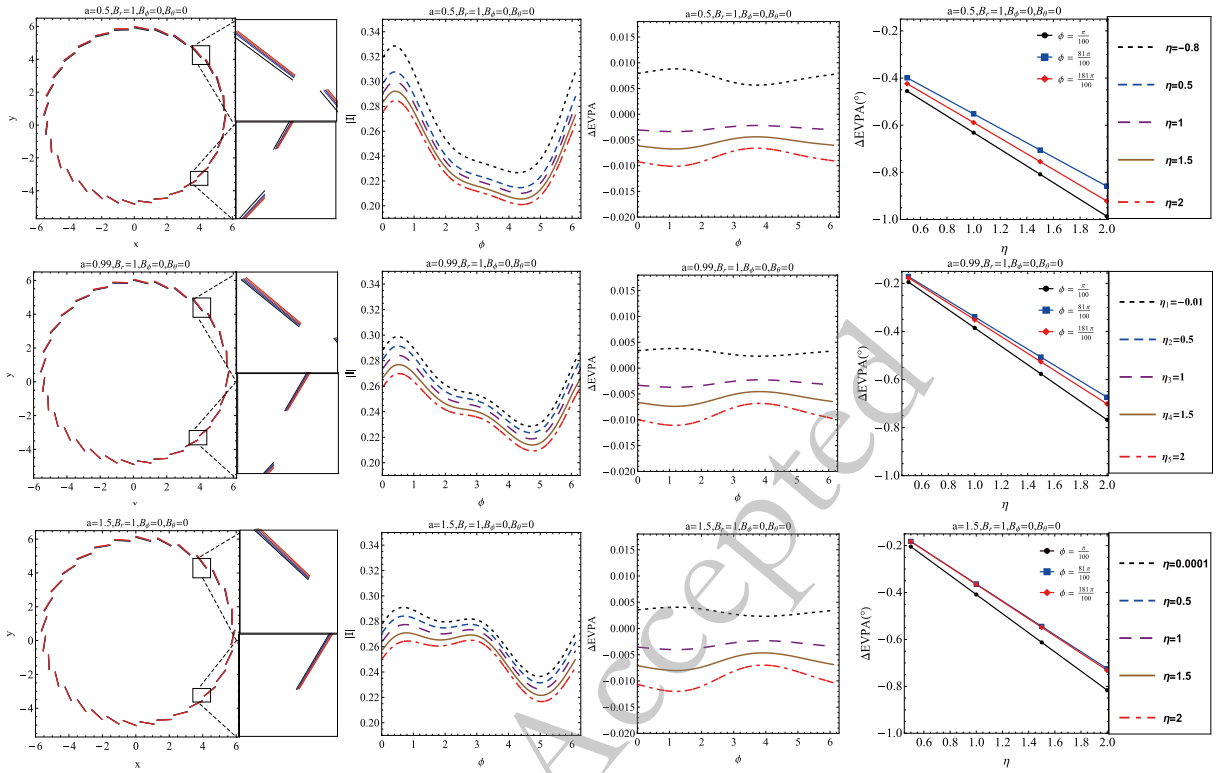

Fig. 1. (color online) Effects of η on the polarization vectors and EVPA in the Konoplya-Zhidenko rotating non-Kerr black hole (1) for different values of a, with an equatorial magnetic field comprising only a radial component B_r. Here, $r_s = 4.5$, $\theta_o = 20°$, $\beta_v = 0.3$, and $\chi = -90°$.

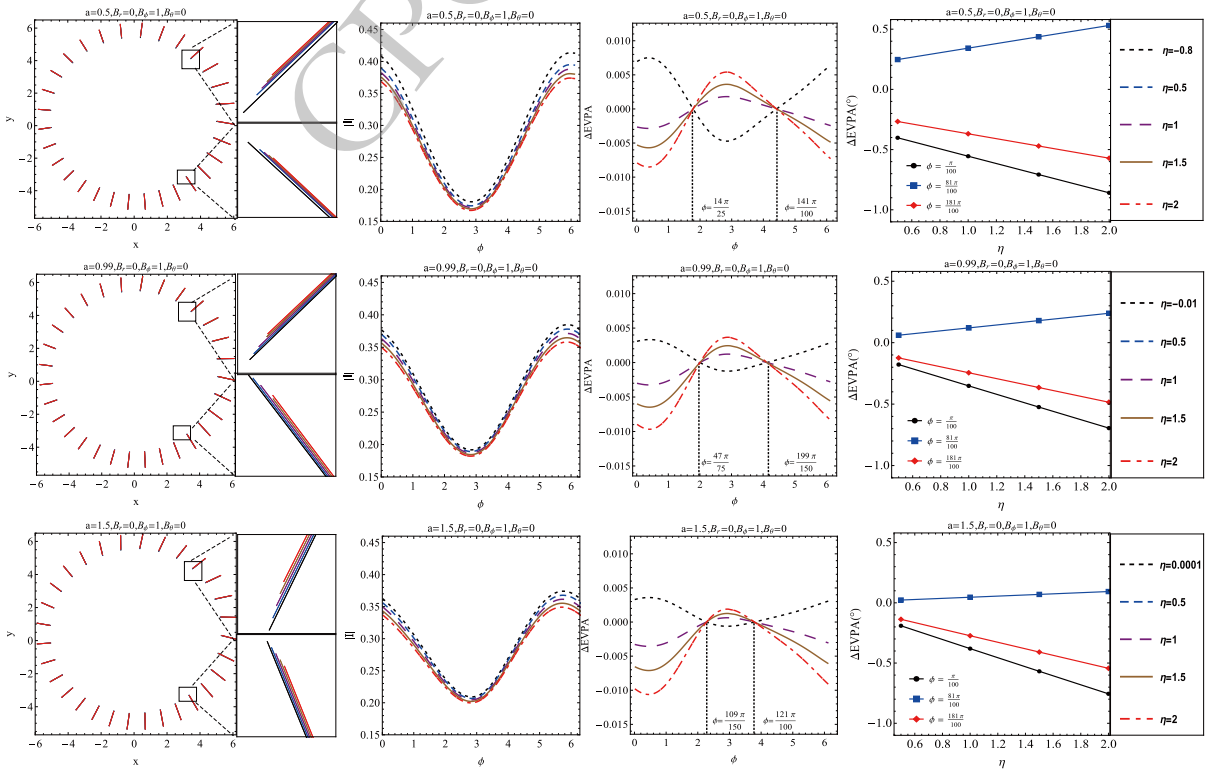

Fig. 2. (color online) Effects of η on the polarization vectors and EVPA in the Konoplya-Zhidenko rotating non-Kerr black hole (1) for various values of a, in the presence of an equatorial magnetic field with only an azimuthal component B_ϕ. Here, $r_s = 4.5$, $\theta_o = 20°$, $\beta_v = 0.3$, and $\chi = -90°$.

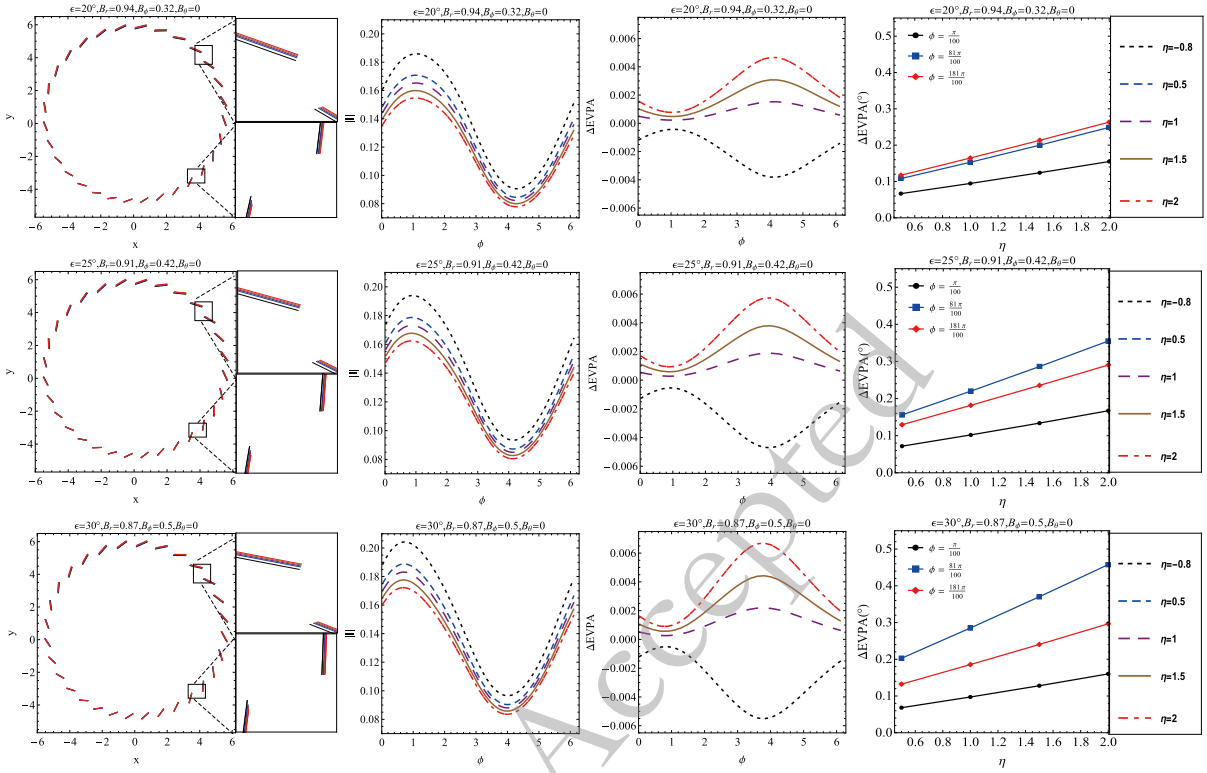

Fig. 3. (color online) Effect of η on the polarization vectors and EVPA in the Konoplya-Zhidenko rotating non-Kerr black hole (1) for different magnetic fields. Here, $r_s = 4.5$, $a = 0.5$, and $\beta_v = 0.3$.

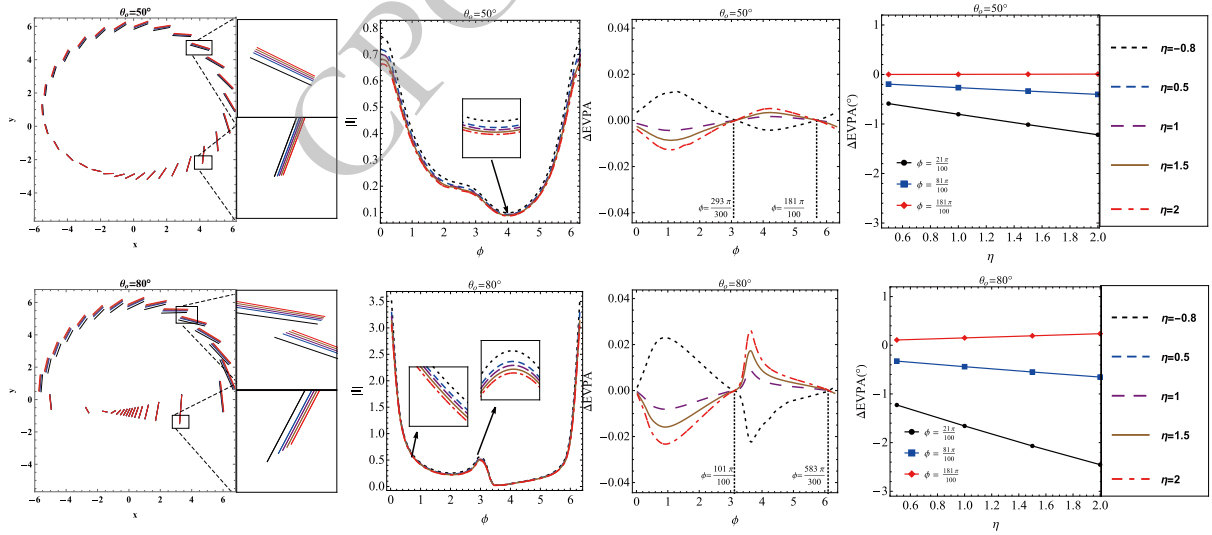

Fig. 4. (color online) Effects of η on the polarization vectors and EVPA in the Konoplya-Zhidenko rotating non-Kerr black hole (1) for various observer inclination angles θ_o. Here, $r_s = 4.5$, $a = 0.5$, $\beta_v = 0.3$, $\chi = -90°$, $B_r = 0.87$, $B_\phi = 0.5$, and $B_\theta = 0$.

Figure 4 presents the polarized images under different magnetic field configurations. As indicated in [11], simulated images in the radially dominated magnetic field regime are more consistent with observations of M87*. Therefore, we focus our analysis on the regime where $B_r > B_\phi$. We find that ΔEVPA increases monotonically with η. Furthermore, for a fixed η, the magnitude of ΔEVPA generally increases with the magnetic field orientation angle. In Fig. 4, we further analyze the polarized images for different observer inclination angles. In the high-inclination regime, the polarization intensity decreases with increasing η. Additionally, the amplitude of variation in the polarization position angle increases significantly with the observer inclination.

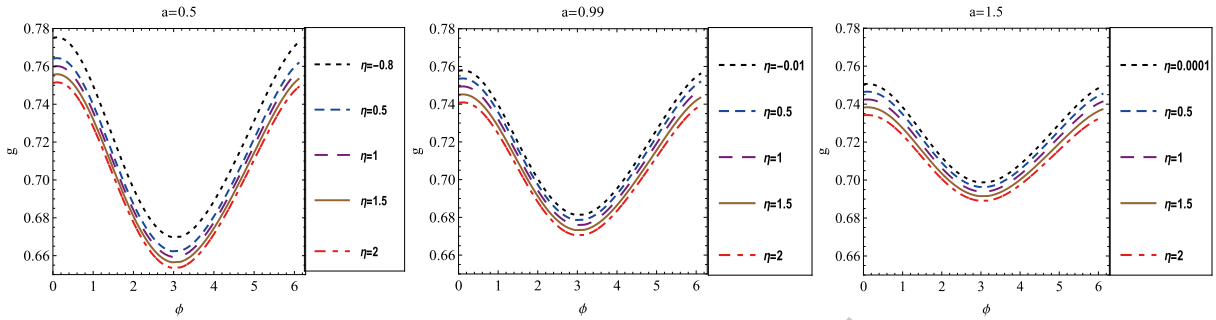

Fig. 5. (color online) Effect of η on the redshift factor g in the Konoplya-Zhidenko rotating non-Kerr black hole metric (1). Here, $r_s = 4.5$ and $\theta_o = 20°$.

Next, we investigate the dependence of ΔEVPA on the deformation parameter η, spin parameter a, and magnetic field orientation angle ϵ at specific azimuthal angles, as illustrated in Fig. 6. The deformation parameter η is positively correlated with ΔEVPA. Notably, the curves for $\phi = 81\pi/100$ and $\phi = 161\pi/100$ nearly coincide, whereas the profile for $\phi = 61\pi/100$ exhibits a distinct separation from the others, indicating a specific sensitivity to the azimuthal angle. In contrast, the spin parameter a induces an overall negative trend in ΔEVPA. A significant separation is observed for the red curve ($\phi = 161\pi/100$), suggesting that a also possesses azimuthal sensitivity, albeit distinct from that of η. Finally, the magnetic field orientation angle ϵ causes an increase in ΔEVPA. The three curves representing different azimuthal angles remain closely clustered, a behavior distinctly different from the impact of η. Although the deformation parameter induces weakly distinguishable azimuthal separation features in ΔEVPA, these subtle signatures are challenging to resolve with current observational capabilities. Future high-resolution facilities, such as the next-generation Event Horizon Telescope (ngEHT), are expected to detect these parameter-specific azimuthal signals.

Finally, we present the Stokes Q–U loops for various spin parameters and magnetic field configurations in Figs. 7–8. The results indicate that, for a fixed observer inclination of $\theta_o = 20°$ and a given magnetic field geometry, both the outer and inner loops contract as the deformation parameter η increases. Assuming a relatively simple magnetic field structure, a larger observed polarization loop supports the hypothesis that the spacetime geometry more closely approximates that of a standard Kerr black hole.

IV. SUMMARY

In this study, we investigate the polarized images of an equatorial emitting ring surrounding a rotating Konoplya-Zhidenko non-Kerr black hole. The results indicate that increasing the deformation parameter η decreases the total polarized intensity. Although the evolution of the EVPA depends on the magnetic field structure, the magnitude of its variation (|ΔEVPA|) consistently increases with η. Furthermore, for a fixed η, the magnitude of ΔEVPA generally increases with the magnetic field orientation angle. Moreover, in the high-inclination regime, the polarization intensity decreases as η increases, whereas the variation amplitude of the polarization position angle increases significantly with the observer inclination.

We also analyze the effects of the deformation parameter η, the spin parameter a, and the magnetic field ori-

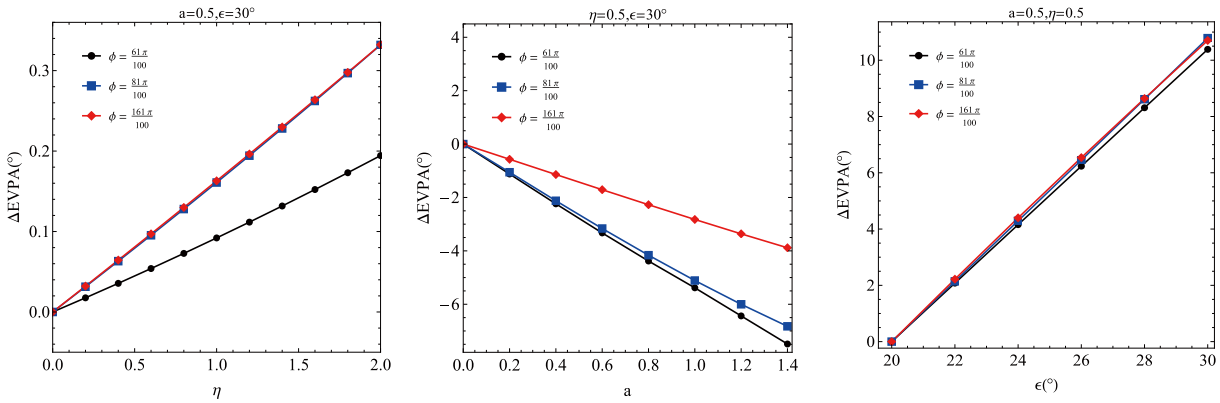

Fig. 6. (color online) The effects of the deformation parameter η (left), the spin parameter a (middle), and the magnetic field orientation angle ϵ (right) on the ΔEVPA. Other parameters are fixed at $r_s = 4.5$ and $\theta_o = 20°$.

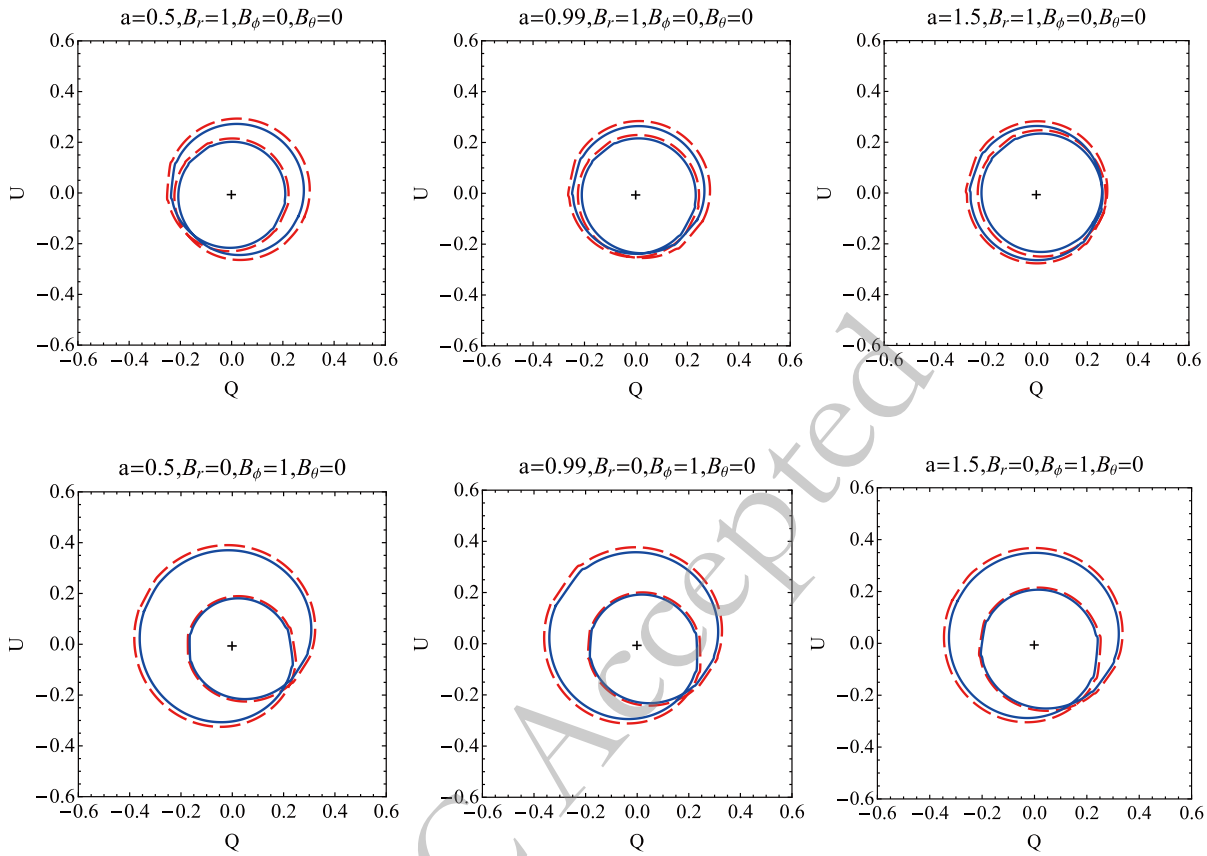

Fig. 7. (color online) Effect of η on the $Q-U$ diagram for various values of a in the Konoplya-Zhidenko rotating non-Kerr black hole (1). We set $r_s = 6$, $\theta_o = 20°$, and $\beta_v = 0.3$. The red dashed and blue solid lines correspond to $\eta = 0.5$ and $\eta = 2$, respectively. The black crosshairs denote the origin of each plot.

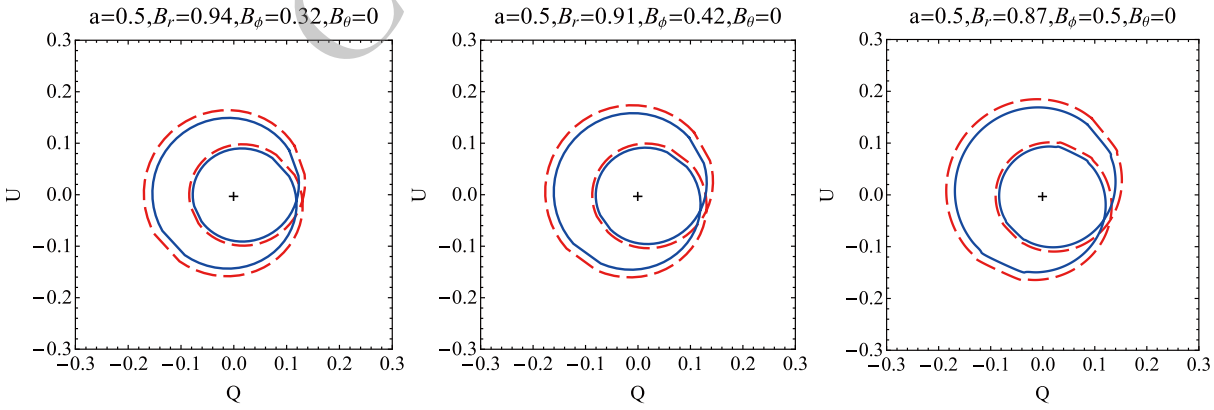

Fig. 8. (color online) Effects of η on the $Q-U$ diagram for different magnetic field structures in the Konoplya-Zhidenko rotating non-Kerr black hole (1). Here, $r_s = 6$, $\theta_o = 20°$, and $\beta_v = 0.3$. The red dashed and blue solid lines represent the cases with $\eta = 0.5$ and $\eta = 2$, respectively. The black crosshairs mark the origin for each plot.

entation angle ϵ on ΔEVPA. The parameter η exhibits a significant positive correlation with ΔEVPA, and its influence displays a distinct azimuthal dependence. In contrast, the spin parameter a causes a general decrease in ΔEVPA, demonstrating a markedly different azimuthal dependence from that of η. Although ϵ increases the magnitude of ΔEVPA, the corresponding curves for different azimuthal angles remain closely clustered. Consequently, the weak yet discernible azimuthal separation induced by η constitutes a unique signature distinguishing its effects from those of a and ϵ, which holds promise for detection by facilities such as the next-generation Event Horizon Telescope (ngEHT). Finally, we investigate the influence of η on the Stokes Q-U loops. Our analysis reveals that

both the outer and inner loop sizes shrink as η increases. This implies that, assuming a relatively simple magnetic field configuration, a larger observed polarization loop suggests a spacetime geometry closer to that of a standard Kerr black hole.

References

[1] Event Horizon Telescope Collaboration, Astrophys. J. Lett. **875**, L1 (2019)
[2] Event Horizon Telescope Collaboration, Astrophys. J. Lett. **875**, L2 (2019)
[3] Event Horizon Telescope Collaboration, Astrophys. J. Lett. **875**, L3 (2019)
[4] Event Horizon Telescope Collaboration, Astrophys. J. Lett. **875**, L4 (2019)
[5] Event Horizon Telescope Collaboration, Astrophys. J. Lett. **875**, L5 (2019)
[6] Event Horizon Telescope Collaboration, Astrophys. J. Lett. **875**, L6 (2019)
[7] Event Horizon Telescope Collaboration, Astrophys. J. Lett. **930**, L12 (2022)
[8] Event Horizon Telescope Collaboration, Astrophys. J. Lett. **875**, L7 (2019)
[9] Event Horizon Telescope Collaboration, Astrophys. J. Lett. **875**, L8 (2019)
[10] Event Horizon Telescope Collaboration, Astrophys. J. Lett. **875**, L9 (2019)
[11] R. Narayan, D. C. M. Palumbo, M. D. Johnson, Z. Gelles, E. Himwich, D. O. Chang, A. Ricarte, J. Dexter, C. F. Gammie, A. A. Chael, and The Event Horizon Telescope Collaboration, Astrophys. J. **912**(1), 35 (2021)
[12] Z. Gelles, E. Himwich, D. C. M. Palumbo, and M. D. Johnson, Physical Review D **104**(4), 044060 (2021)
[13] X. Qin, S. Chen, and J. Jing, Eur. Phys. J. C **82**, 784 (2022)
[14] Z. Hu, Y. Hou, H. Yan, M. Guo, and B. Chen, Eur. Phys. J. C **82**, 1166 (2022)
[15] X. Qin, S. Chen, Z. Zhang, and J. Jing, Eur. Phys. J. C **83**, 159 (2023)
[16] H. Zhu and M. Guo. *arxiv*, page 2205.04777, 2023.
[17] Y. Hou, J. Huang, M. Guo, Y. Mizuno, and B. Chen, Astrophys. J. Lett. **988**, L51 (2025)
[18] F. Zhou, J. Huang, Y. Li, Z. Zhang, Y. Hou, M. Guo, and B. Chen. *arxiv*, page 2512.06803, 2025.
[19] V. Deliyski, G. Gulychev, P. Nedkova, and S. Yazadjiev, Phys. Rev. D **108**, 104049 (2023)
[20] S. Gu, Y. Huang, K. Liu, E. Liang, and K. Lin, Eur. Phys. J. C **84**, 601 (2024)
[21] H. Shi and T. Zhu, Eur. Phys. J. C **84**, 814 (2024)
[22] Y. Chen, L. Cheng, P. Wang, and H. Yang. *arxiv*, page 2409.05304, 2024.
[23] C. Chen, Q. Pan, and J. Jing. *J. Cosmol. Astropart. P.*, 04: 024.
[24] T. Johannsen and D. Psaltis, Phys. Rev. D **83**, 124015 (2011)
[25] R. Konoplya and A. Zhidenko, Phys. Lett. B **756**, 350 (2016)
[26] C. Bambi and S. Nampalliwar, Europhys. Lett. **130**, 10006 (2020)
[27] Y. Ni, J. Jiang, and C. Bambi, J. Cosmol. Astropart. P. **09**, 014 (2016)
[28] S. Wang, S. Chen, and J. Jing, J. Cosmol. Astropart. P. **11**, 020 (2016)
[29] M. Wang, S. Chen, and J. Jing, J. Cosmol. Astropart. P. **01**, 051 (2017)
[30] F. Long, S. Chen, S. Wang, and J. Jing, Nucl. Phys. B **926**, 1 (2018)
[31] F. Long, S. Wang, S. Chen, and J. Jing, Eur. Phys. J. C **85**, 26 (2025)
[32] K. He, C. Yang, and X. Zeng. *arxiv*, page 2501.06778, 2025.
[33] S. E. Gralla and A. Lupsasca, Phys. Rev. D **101**, 044031 (2020)
[34] E. Himwich, M. D. Johnson, A. Lupsasca, and A. Strominger, Phys. Rev. D **101**(2), 084020 (2020)
[35] M. Walker and R. Penrose, Commun. Math. Phys. **118**, 265 (2001)
[36] S. Chandrasekhar. *The Mathematical Theory of Black Holes*. Oxford University Press, 1985.